

Constrained Bayesian Optimization Using a Lagrange Multiplier Applied to Power Transistor Design

Ping-Ju Chuang,¹ Ali Saadat,² Sara Ghazvini,¹ Hal Edwards,³ and William G. Vandenberghe¹

¹*Department of Materials Science and Engineering, The University of Texas at Dallas, Richardson, TX 75080 USA*

²*Kilby Labs, Texas Instruments Inc., Santa Clara, CA 95051 USA*

³*Analog Technology Development, Texas Instruments Inc., Dallas, TX 75243 USA*

(*Electronic mail: william.vandenberghe@utdallas.edu.)

We propose a novel constrained Bayesian Optimization (BO) algorithm optimizing the design process of Laterally-Diffused Metal-Oxide-Semiconductor (LDMOS) transistors while realizing a target Breakdown Voltage (BV). We convert the constrained BO problem into a conventional BO problem using a Lagrange multiplier. Instead of directly optimizing the traditional Figure-of-Merit (FOM), we set the Lagrangian as the objective function of BO. This adaptive objective function with a changeable Lagrange multiplier can address constrained BO problems which have constraints that require costly evaluations, without the need for additional surrogate models to approximate constraints. Our algorithm enables a device designer to set the target BV in the design space, and obtain a device that satisfies the optimized FOM and the target BV constraint automatically. Utilizing this algorithm, we have also explored the physical limits of the FOM for our devices in 30 - 50 V range within the defined design space.

I. INTRODUCTION

Efficient power electronics are an essential component of a society powered by renewable energy. Power semiconductor devices have been extensively adapted in all applications that require electrical power. Different materials such as silicon¹, Silicon carbide (SiC)^{2,3}, and Gallium nitride (GaN)^{4,5}, along with various device structures like power diodes, planar/trench Metal-Oxide-Semiconductor Field-Effect Transistors (MOSFETs)^{6,7}, and Insulated-Gate Bipolar Transistors (IGBTs)^{8,9}, are utilized in the fabrication of a wide range of analog microchips, catering to the power needs of diverse power management applications. The choice of material and device structure depends on the operating voltage requirements and specific performance characteristics desired for each application. These technologies enable the provision of electrical power to various appliances and systems. Among all power semiconductor devices, silicon-based Laterally-Diffused Metal-Oxide-Semiconductor (LDMOS) transistors are the most popular device since they can be seamlessly integrated into Integrated Circuit (IC) technology¹⁰⁻¹⁶, bringing economic benefits and being able to bridge an extensive voltage range.

The Figure-of-Merit (FOM) = $BV^2/R_{sp(on)}$ is an important metric employed to assess the quality of power devices¹⁷. This criterion reflects the maximum achievable power density in a power device which is crafted by specific materials. As the LDMOS transistor is integrated within the silicon process and widely used to design various devices working at different operating voltages, the design challenge for LDMOS transistors has shifted to minimize the $R_{sp(on)}$ at specific voltages to approach the material's physical limits and reduce the cost simultaneously. This principle of device design, known as the "power density scaling" law has been consistently applied in the field of power device design. Following this law, consequently, the ongoing challenge in the industry lies in designing and optimizing different LDMOS transistors with disparate BV values within the same semiconductor process.

In Moore's Law transistors, all parameters such as the operation voltage are chosen for accurate and efficient communication, aiming to reduce cost-per-transistor for every new technology node¹⁸. In power semiconductor technology, however, microchips process power flows across different voltage domains specific to each application. For instance, a laptop power converter must efficiently convert direct current (DC) power from a 12 V battery to drive a 1 V microprocessor. Similarly, automotive applications may require transient operation at 40 V or higher due to fault conditions which exist in the automotive environment. Power transistors must support a wide voltage range, and their breakdown voltage (BV) needs to be substantially higher than the operating voltage to ensure reliability throughout their operation lifetime. For example, the laptop 12 V to 1 V DC power converter mentioned above may require $BV > 30$ V, whereas an automotive microchip that survives fault conditions at 40 V might need a device with $BV > 55$ V. Thus, the optimization of power transistors involves selecting a limited range of BV values, considering specific application requirements.

Bayesian optimization (BO) is a data-driven algorithm that efficiently determines the global extremum within a defined space while minimizing the number of evaluations required^{19,20}. In recent years, BO has gained significant popularity as a replacement for grid search or random search in optimizing the architecture of different machine learning models²¹⁻²³. Moreover, BO is being increasingly adopted in various research domains to accelerate the optimization process and enhance the development of their respective fields such as chemical synthesis²⁴, process of solar cells²⁵, optimization of lithium-ion batteries²⁶, and drug discovery²⁷. Ironically, in more mature fields like the semiconductor industry, due to its earlier development compared to the popularity of BO, there is relatively less use of BO or other artificial intelligence assisted tools. We have previously integrated different optimization algorithms with Technology computer-aided design (TCAD) simulations to automate the optimization of semiconductor devices²⁸. Among all these optimization algo-

gorithms, BO is the most data efficient method to integrate with TCAD device simulations.

TCAD simulation is an indispensable tool in semiconductor device manufacturing. Due to the high cost associated with semiconductor device fabrication, performing TCAD simulations and designing desired device characteristics is a crucial part of device fabrication. Skilled engineers perform a large number of TCAD simulations, often guided by design of experiments (DOE) approaches like factorial designs, response surface designs, or Taguchi designs^{29,30}. The combination of DOE and TCAD simulations requires significant manual intervention and human involvement in the process. By integrating BO with TCAD simulations, we can perform automated and globally optimized designs, accelerating the development process. However, while optimizing device design, constraints must be respected. e.g., when designing a power device, BV needs to be sufficiently high. Checking whether a constraint (BV) is satisfied can be the most computationally expensive part of simulations. Previous constrained BO relies on different surrogate models to approximate both the output parameter (BV) and the objective function (FOM)³¹. However, this approach requires using multiple surrogate models, which increase the time and resources required for evaluations to solve such constrained BO problems.

In this paper, we propose a constrained BO process using a Lagrange multiplier. We apply the methodology to the optimization of an LDMOS transistors enabling the optimization of LDMOS transistors with a given breakdown voltage. We first show that the unconstrained BO yields a device with a breakdown voltage of 31 V but reveals no information about devices with BV of 40 V or 50 V. Next, we show that we can successfully constrain the BV and find high-FOM devices for $BV = 40$ V and $BV = 50$ V. Our results demonstrate that constrained BO can effectively accomplish the optimization of device designs with specific BV restrictions, and even explore the physical limits for a specific breakdown voltage range without requiring human intervention.

II. RESULTS

The LDMOS transistors under investigation are illustrated in Fig. 1. We use the standard Gaussian doping setting in the commercial simulation software to define all the doping profiles in this study³². The elongated-diamond-shaped oxide region on the top of the device represents a Local-Oxidation Structure (LOCOS). The LOCOS acts as a field-relief oxide and increases the breakdown voltage when designed appropriately. The Junction Field-Effect-Transistor (JFET) region is located on the drift region which is not covered by the LOCOS. The fabrication process of LDMOS transistors with LOCOS can be found on Ref.³³. The doping concentration in the channel is chosen so that the leakage current remains smaller than 10^{-13} A/ μ m. The device under consideration has 19 parameters to define the device structure. For the BO, we optimize nine input parameters while keeping ten other input parameters fixed. For detail about constructing LDMOS transistors with LOCOS by 19 parameters in TCAD, we refer to the

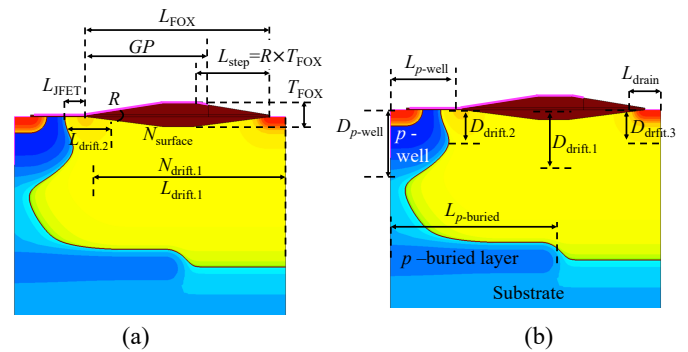


FIG. 1. Schematic cross-section of an LDMOS with elongated diamond LOCOS. (a) nine input parameters and (b) ten fixed parameters are labeled. TABLE I lists nine input parameters and their bounds.

subsection IV A 1.

The FOM = $BV^2/R_{sp(on)}$ is the objective function of our unconstrained BO. BV , $R_{sp(on)}$, and FOM are illustrated in the methodology section. The first 10 device configurations are chosen randomly followed by 190 or 790 new device structures generated iteratively using the acquisition function which maximizes the expected improvement of the FOM or the Lagrangian. Gaussian process regression is used to emulate the ground truth response surface in our design space. We first show the results of an unconstrained BO, followed by a constrained BO by developing a Lagrangian approach, finally we determine the frontier of the FOM vs BV .

Fig. 2 (a) exhibits the FOM and BV for 200 devices simulated in an unconstrained BO. The color of each marker indicates the order in which the devices are simulated with the darkest blue device simulated first, and the brightest red device simulated last. Most of the devices that are simulated last are found near the device with the highest FOM = 295 kW/mm². This highest FOM device is found to have $BV = 31$ V. The vast majority of simulated devices have a $BV < 31$ V, a few high FOM devices are identified with $BV \approx 35$ V while no high-FOM devices with $BV > 40$ V are simulated during the BO. For applications requiring $BV > 40$ V, the unconstrained FOM does not provide insight in device design.

Fig. 2 (b) and (c) present 200 devices simulated in a constrained optimization with the target $BV = 40$ and 50 V constraints respectively. For the constrained BO, we use the same approach as for the unconstrained BO except that we optimize a Lagrangian function as detailed in the method section. Fig. 2 (b) has a maximum FOM = 270 kW/mm² at $BV = 41$ V while Fig. 2 (c) has identified a FOM = 207 kW/mm² device with a $BV = 50$ V. The device with FOM = 207 kW/mm² at $BV = 50$ V is not the highest FOM device simulated in Fig. 2 (c) but it is the highest FOM device that can realize a 50 V breakdown voltage. Looking visually at the distribution of the devices in Fig. 2 (a) - (c), by adding the Lagrange term, many more devices with higher BV are simulated.

Fig. 3 reveals the frontier of FOM vs BV . We obtain the device configurations in Fig. 3 by performing a constrained BO where the constraint is changed at every iteration step. In

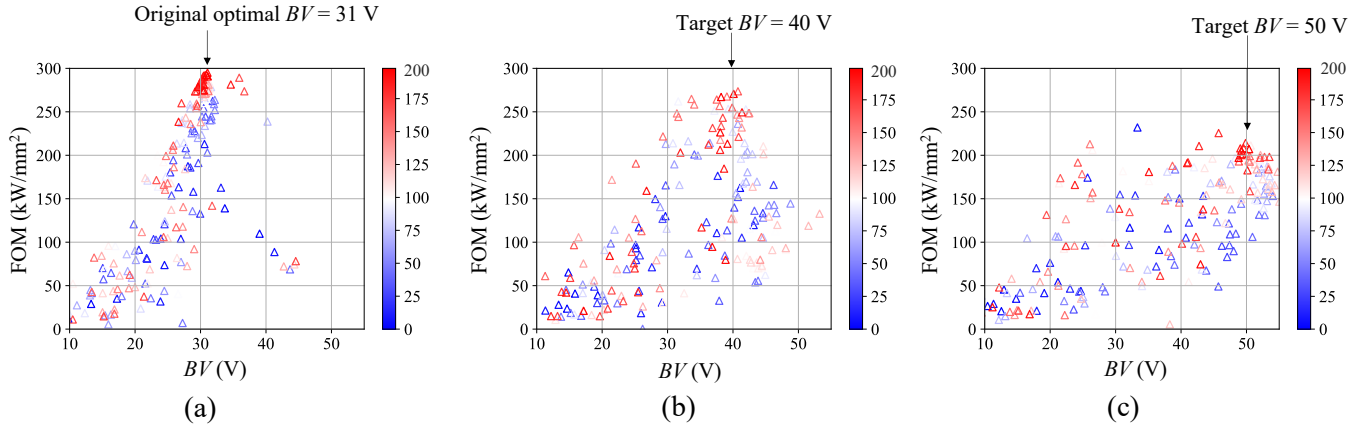


FIG. 2. The BO result (a) without any constraint (b) with a constrained target $BV = 40$ V, (c) constrained $BV = 50$ V. The color bar indicates the progress of the BO. A deeper red color means the data point is simulated closer to the final step. Fig. 2(b-c) indicate that by performing a constrained optimization, the optimization result changed from the original optimal $BV = 31$ V to the constrained target $BV = 40$ V and 50 V.

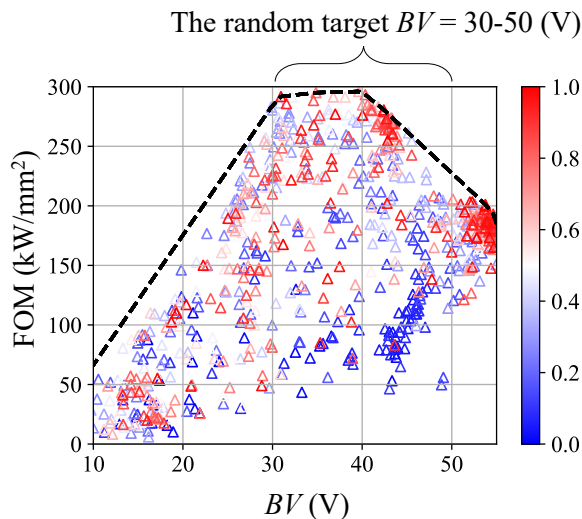


FIG. 3. The upper boundary shows the physical limitation of FOM for LDMOS transistors with LOCOS in our design space. We perform 800 simulations and assign target BV randomly between 30 - 50 V in each iteration.

each iteration, a target BV is chosen randomly between 30 V and 50 V and the acquisition function chooses a new design based on the Lagrange multiplier associated with the target BV of the current iteration and all previously acquired FOM and BV data. A total of 800 devices are simulated and the upper hull of the obtained results is indicated. Interestingly, the device with the highest FOM = 299 kW/mm^2 is found to have a $BV = 40$ V, exceeding the best device we found from the unconstrained BO with 200 iterations in Fig. 2 (a). Within the design space that we have defined, we find that FOM ≈ 300 kW/mm^2 devices can be designed with a $BV = 30$ V to $BV = 40$ V. Devices with a BV up to 55 V can be designed but the FOM would decrease to ≈ 200 kW/mm^2 .

Fig. 4 (a) - (c) elucidate the device operation of the highest FOM device from the unconstrained BO, the constrained BO with $BV = 40$ V and $BV = 50$ V respectively. The figures on the upper row exhibit the doping profile, while the figures on the lower row are electrical field distributions at the breakdown condition. Inspecting the highest FOM device in the unconstrained BO, we find that the BO drives the device structure result on a diamond-shaped LOCOS as illustrated in Fig. 4 (a) compared to the elongated diamond-shapes in Fig. 4 (b) - (c). However, when constraining the BV to 40 V or 50 V, elongated-diamond shape devices are identified as having the highest FOM. Moreover, the results obtained from these algorithms align with the physical intuition of designers. For example, a higher BV device requires a lower drift doping concentration. The BO enables the automatic identification of which overall structure yields the highest FOM, without relying on time-consuming local/manual optimization.

III. DISCUSSION

Comparing the results in Fig. 2 and 3, we observe that for the 30 V optimized device, the FOM results are almost identical. However, when comparing the 40 V optimized device designs, we can see that the FOM in Fig. 2 (b) is approximately 270 kW/mm^2 , while it is around 299 kW/mm^2 in Fig. 3. The higher FOM obtained in Fig. 3 is not entirely surprising because 800 iterations were used in Fig. 3 compared to the 200 for Fig. 2. Seemingly, the 30 V BV region is easier to access for the BO compared to the 40 V region. Nevertheless, from our study it appears that an informed constrained optimization can aid BO.

By adding a Lagrange multiplier to the BO, we have successfully been able to perform constrained BO. Specifically, using TCAD simulations, we have effectively been able to constrain the BV . Our problem is a specific example of a constraint that requires resource-intensive measurements or evaluations. A previous approach to constrained BO added

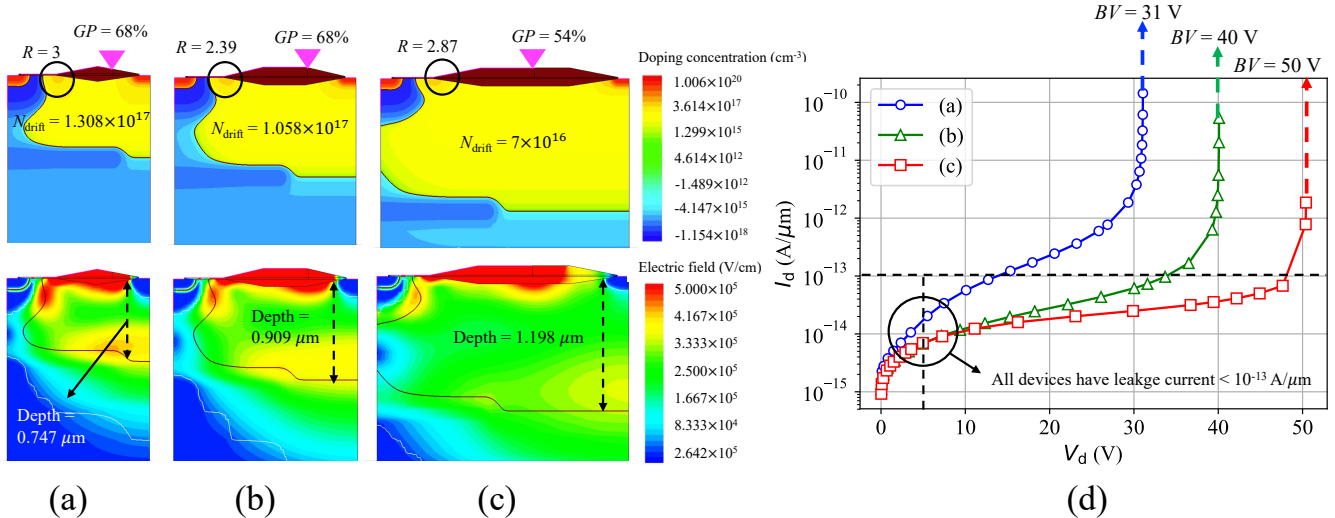


FIG. 4. The doping profile and the electrical field distribution for optimized device with (a) $BV = 31$ V from the unconstrained BO framework, (b) $BV = 40$ V from our novel algorithm, (c) $BV = 50$ V from our novel algorithm. (d) Breakdown curves for the three devices.

an additional surrogate function to approximate the output³¹, but in this approach, as the number of constrained output variables increases, more surrogate functions are needed to approximate each output individually. Our constrained BO algorithm is able to solve the specific design problem without any additional computational cost.

IV. METHODS

A. TCAD simulation

1. Device structure simulation

In Fig. 1 (a) Nine parameters are adjustable as input parameters for our TCAD simulations. 1) the peak doping concentration ($x_1 = N_{\text{drift.1}}$) of the first Gaussian doping, 2) the length of the first Gaussian doping peak line ($x_2 = L_{\text{drift.1}}$), 3) the length of the second Gaussian doping peak line ($x_3 = L_{\text{drift.2}}$), 4) the gate position ($x_4 = GP$), 5) the length of the JFET region ($x_5 = L_{\text{JFET}}$), 6) the length of the FOX ($x_6 = L_{\text{FOX}}$), 7) the doping concentration value on the surface of drift region ($x_7 = N_{\text{surface}}$), 8) the thickness of the FOX ($x_8 = T_{\text{FOX}}$), 9) the shape ratio of LOCOS ($x_9 = R$). Among these input parameters, $L_{\text{drift.1}}$, $L_{\text{drift.2}}$, GP , L_{JFET} , L_{FOX} are layout related parameters which can be defined by photo masks. Nevertheless, $N_{\text{drift.1}}$, N_{surface} , T_{FOX} , R are process related input parameters. The n -type dose for the first Gaussian doping determines $N_{\text{drift.1}}$ and N_{surface} . The local oxidation process determines T_{FOX} and R . The shape ratio (R) is defined to be equal to $L_{\text{step}}/T_{\text{FOX}}$, where L_{step} is the taper length of LOCOS. R is used to describe the shape of the bird's beak which has significant impact on the performance of the LDMOS transistors. The larger R causes a slender and elongated beak, whereas a smaller R yields a shorter and stout beak. Therefore, various shapes of field ox-

TABLE I. Symbols, descriptions, and bounds of the nine input parameters for the BO

Symbol (units)	Description	Bound
$N_{\text{drift.1}}$ (cm^{-3})	The peak value of the 1 st Gaussian doping	7×10^{16} - 2.5×10^{17}
$L_{\text{drift.1}}$ (nm)	The length of the 1 st Gaussian doping	250 - 2700
$L_{\text{drift.2}}$ (nm)	The length of the 2 nd Gaussian doping	0 - 500
GP (%)	Percentage of the FOX covered by the gate	10 - 99
L_{JFET} (nm)	The length of JFET region	0 - 700
L_{FOX} (nm)	The length of field oxide (FOX)	750 - 2000
N_{surface} (cm^{-3})	The doping concentration value on the surface of the drift region	1×10^{16} - 6×10^{16}
T_{FOX} (nm)	The thickness of the FOX	50 - 150
R	The tangent of the angle of the FOX	0.5 - 5

ide structures and doping profiles are considered in our simulations.

Fig. 1 (b) illustrates the fixed parameters during the optimization. We use a uniform p -type with $2 \times 10^{16} \text{ cm}^{-3}$ doping concentration as the substrate. A p -type buried layer with a doping concentration of $9 \times 10^{16} \text{ cm}^{-3}$ is introduced. The length of the p -buried layer is fixed to $L_{p\text{-buried}} = 0.95 \mu\text{m}$. A high p -type doping concentration of $2 \times 10^{18} \text{ cm}^{-3}$ is applied on the surface as the p -well for the LDMOS with a fixed depth $D_{p\text{-well}} = 0.4 \mu\text{m}$ and a fixed length $L_{p\text{-well}} = 0.1 \mu\text{m}$. The first drift Gaussian doping peak is positioned at a depth of $0.3 \mu\text{m}$, forming the primary drift region. The second n -type

doping has a doping concentration of $N_{\text{drift},2} = 5 \times 10^{17} \text{ cm}^{-3}$, creating the channel in cooperation with the p -well. The third n -type doping is located beneath the drain region, and it shares the same doping concentration as the second n -type doping. This arrangement serves to reduce the gradient of the doping concentration between the drain and the primary drift region so that the electric field on the drain side can be decreased. The thin gate oxide thickness is 12 nm. A LOCOS is implemented on top of the main drift region to increase the BV of the LDMOS transistors. The gate is placed on the elongated-diamond, allowing for the application of gate voltage stress on both the p -well and the drift region to control the channel in on-state and electric field distribution on the device surface in off-state. The source and drain regions, featuring an n -type doping concentration of $2 \times 10^{20} \text{ cm}^{-3}$, are positioned at the two terminals of the device with a same length $L_{\text{source}} = L_{\text{drain}} = 0.1 \mu\text{m}$. The definition of the half-pitch as the distance between the source and drain.

We minimize the number of input parameters in order to simplify the complexity of the TCAD simulation. Some parameters are dependent on defined input parameters. The depth of the drift region (D_{drift}) is determined by the doping concentration value on the surface of the drift region (N_{surface}) and the peak value of the first Gaussian doping ($N_{\text{drift},1}$) since the first doping profile is a Gaussian distribution. The depth of the drift region is equaling to

$$D_{\text{drift}} = 0.3\mu\text{m} + 3\sqrt{\frac{0.045}{\ln(N_{\text{drift},1}/N_{\text{surface}})}}\mu\text{m}. \quad (1)$$

The thickness of the LOCOS (T_{FOX}) and the shape of tangent of the angle of the FOX (R) determines the taper length of LOCOS (L_{step}) in Fig.1 (a) through $L_{\text{step}} = T_{\text{FOX}} \times R$.

2. TCAD Physical Models

For our simulations, we utilize a commercial drift-diffusion software with default silicon parameters³². To accurately capture various physical mechanisms, we use generation-recombination model, including the doping-dependent and the temperature-dependent Shockley-Read-Hall model, and the Auger model, each addressing specific aspects of carrier behavior and recombination processes. The van Overstraeten model³⁴ is used to account for the impact ionization process. To account for mobility degradation at the silicon-insulator interface, we employ the Lombardi model. In the bulk region, we utilize the widely accepted Philips unified mobility model, which provides a comprehensive description of carrier mobility. Carrier distributions are modeled using the Fermi-Dirac distribution, including the bandgap narrowing model.

3. Device Characteristics

We define the breakdown voltage ($BV(\mathbf{x})$) and the specific on-resistance ($R_{\text{sp(on)}}(\mathbf{x})$). BV represents the maximum voltage between the source and drain that the device can sustain

without experiencing avalanche breakdown when it is in the off-state. We perform the I_d - V_d measurement and ramp up the V_{DS} to extract the maximum V_{DS} when the TCAD no longer converges:

$$BV(\mathbf{x}) = \max(V_{\text{DS}}), \quad \text{when } V_{\text{GS}} = V_{\text{BS}} = V_{\text{SS}} = 0 \text{ V}. \quad (2)$$

We calculate the specific on-state resistance ($R_{\text{sp(on)}}(\mathbf{x})$) by

$$R_{\text{sp(on)}}(\mathbf{x}) = R_{\text{ds(on)}}(\mathbf{x}) \times \text{AREA} \quad (3)$$

where $AREA$ is half-pitch (HP) times a unit length (default value is $1 \mu\text{m}$ on the z -direction since we are performing 2D simulations) and $R_{\text{ds(on)}}(\mathbf{x}) = V_{\text{DS}}(\mathbf{x})/I_{\text{DS}}(\mathbf{x})$, when $V_{\text{GS}} = 5 \text{ V}$ and $V_{\text{DS}} = 0.1 \text{ V}$. We defined the current between source and drain as the leakage current when $V_{\text{GS}} = 0 \text{ V}$ and $V_{\text{DS}} = 5 \text{ V}$. The leakage current is defined at $V_{\text{DS}} = 5 \text{ V}$ in order to simplify the simulation process and shorten the simulation time. We fixed the p -well doping profile and the second drift doping so that the channel length and the leakage current is fixed in all of our devices. All of our devices exhibit a leakage current less than $10^{-13} \text{ A}/\mu\text{m}$. Leakage current is not the focus of our present study and could be further improved by adjusting the doping concentration of p -well and the second Gaussian doping in the drift region.

Lastly, the FOM is the most important metric in this study, equaling

$$\text{FOM}(\mathbf{x}) = \frac{BV(\mathbf{x})^2}{R_{\text{sp(on)}}(\mathbf{x})}. \quad (4)$$

B. Bayesian Optimization

For details of BO, we refer to^{19,20}. We utilize the open-source package, *skopt*. We use Gaussian Process Regression (GPR) as the surrogate model and the Expected Improvement (EI) as the acquisition function. The radial basis function (RBF) kernel with length 1.0 is used in the GPR. For the acquisition function, the Limited-memory Broyden-Fletcher-Goldfarb-Shanno (L-BFGS) algorithm is used and 20 iterations are executed to find the extremum of the acquisition function.

C. Lagrange Multiplier

The algorithm flow chart for the constrained BO problem is shown in Fig. 5. The objective function of the BO is the Lagrangian

$$\mathcal{L}(\mathbf{x}, \lambda) = f(\mathbf{x}) + \lambda g(\mathbf{x}) = \text{FOM}(\mathbf{x}) + \lambda(BV - BV_{\text{target}}) \quad (5)$$

where λ is the Lagrange multiplier. In our specific problem $f(\mathbf{x}) = \text{FOM}(\mathbf{x})$ and $g(\mathbf{x}) = BV - BV_{\text{target}}$. The Lagrangian function reaches its optimum when $g(\mathbf{x}) = 0$. Note that when optimizing, BV_{target} is a constant and once λ is determined, the last term $-\lambda BV_{\text{target}}$ in Eq. (5) is just a constant which can be

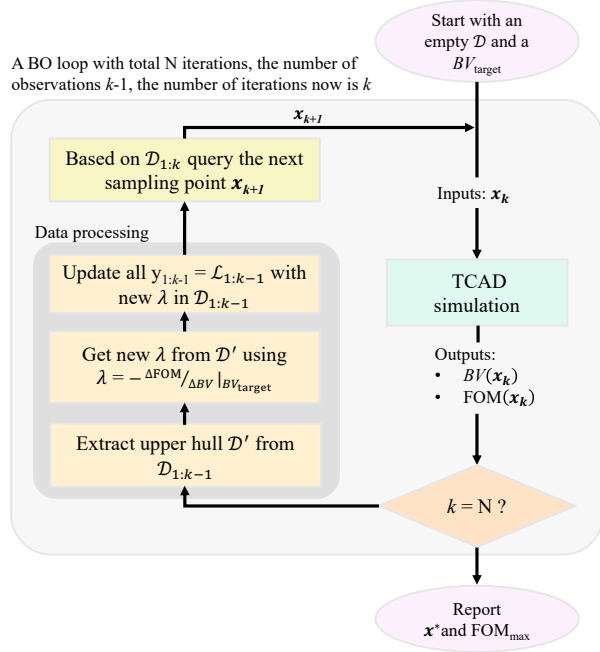


FIG. 5. The optimization flow for constrained optimization algorithm. The Lagrange multiplier for the next iteration is determined from the dataset of simulated devices. The λ for the first two iterations is set to 0.

omitted without affecting the results. Correctly determining the Lagrange multiplier λ is critical.

We compute the Lagrange multiplier from the simulated data. We determine the devices that form the upper part of the convex hull that contains the FOM vs BV data, yielding a dataset $\mathcal{D}' = \{(BV_i, FOM_i)\}$, where i is an index iterating over the data in the upper hull. The upper hull is illustrated in Fig. 3 where the upper part of the hull consists of a set of 5 points ($i = 1 - 5$). We then identify in which segment of the upper hull the target BV is located, *i.e.* $BV_j < BV_{\text{target}} < BV_{j+1}$, where j is the number of the segments in the upper hull curve. Finally, the Lagrange multiplier is determined as

$$\lambda = - \left. \frac{\Delta f}{\Delta g} \right|_{BV_{\text{target}}} = - \frac{FOM_{j+1} - FOM_j}{BV_{j+1} - BV_j}. \quad (6)$$

ACKNOWLEDGMENTS

The author also appreciates all of valuable discussion with Dr. Sujatha Sampath of Texas Instruments.

DATA AVAILABILITY STATEMENT

The data that support the findings of this study are available on request from the corresponding author.

¹B. J. Baliga, *Fundamentals of Power Semiconductor Devices* (Springer Science & Business Media, 2010).

²T. Kimoto and J. A. Cooper, *Fundamentals of Silicon Carbide Technology: Growth, Characterization, Devices and Applications* (John Wiley & Sons, 2014).

³X. She, A. Q. Huang, O. Lucia, and B. Ozpineci, "Review of Silicon Carbide Power Devices and Their Applications," *IEEE Transactions on Industrial Electronics* **64**, 8193–8205 (2017).

⁴M. Meneghini, C. De Santi, I. Abid, M. Buffolo, M. Cioni, R. A. Khadar, L. Nela, N. Zagni, A. Chini, F. Medjdoub, *et al.*, "GaN-based Power Devices: Physics, Reliability, and Perspectives," *Journal of Applied Physics* **130** (2021).

⁵K. J. Chen, O. Häberlen, A. Lidow, C. I. Tsai, T. Ueda, Y. Uemoto, and Y. Wu, "GaN-on-Si Power Technology: Devices and Applications," *IEEE Transactions on Electron Devices* **64**, 779–795 (2017).

⁶R. K. Williams, M. N. Darwish, R. A. Blanchard, R. Siemieniec, P. Rutter, and Y. Kawaguchi, "The Trench Power MOSFET: Part I — History, Technology, and Prospects," *IEEE Transactions on Electron Devices* **64**, 674–691 (2017).

⁷R. K. Williams, M. N. Darwish, R. A. Blanchard, R. Siemieniec, P. Rutter, and Y. Kawaguchi, "The Trench Power MOSFET — Part II: Application Specific VDMOS, LDMOS, Packaging, and Reliability," *IEEE Transactions on Electron Devices* **64**, 692–712 (2017).

⁸N. Iwamuro and T. Laska, "IGBT History, State-of-the-Art, and Future Prospects," *IEEE Transactions on Electron Devices* **64**, 741–752 (2017).

⁹V. K. Khanna, *Insulated Gate Bipolar Transistor IGBT Theory and Design* (John Wiley & Sons, 2004).

¹⁰S.-Y. Chen, B. Liao, J.-C. Dong, T. Wang, S.-L. Wang, H.-Y. Yang, Y.-W. Peng, S.-C. Huang, and J.-Y. Gan, "Study on 20 V LDMOS with Stepped-Gate-Oxide Structure for PMIC Applications: Design, Fabrication, and Characterization," *IEEE Transactions on Electron Devices* **69**, 878–881 (2021).

¹¹H.-L. Chou, P. Su, J. Ng, P. Wang, H. Lu, C. Lee, W. Syue, S. Yang, Y. Tseng, C. Cheng, *et al.*, "0.18 μm BCD Technology Platform with Best-in-Class 6 V to 70 V Power MOSFETs," in *2012 24th International Symposium on Power Semiconductor Devices and ICs* (IEEE, 2012) pp. 401–404.

¹²F. Jin, D. Liu, J. Xing, X. Yang, J. Yang, W. Qian, W. Yue, P. Wang, M. Qiao, and B. Zhang, "Best-in-Class LDMOS with Ultra-Shallow Trench Isolation and p -buried Layer from 18 V to 40 V in 0.18 μm BCD Technology," in *2017 29th International Symposium on Power Semiconductor Devices and IC's (ISPSD)* (IEEE, 2017) pp. 295–298.

¹³T.-Y. Huang, W.-Y. Liao, C.-Y. Yang, C.-H. Huang, W.-C. V. Yeh, C.-F. Huang, K.-H. Lo, C.-W. Chiu, T.-C. Kao, H.-D. Su, *et al.*, "0.18 μm BCD Technology with Best-in-Class LDMOS from 6 V to 45 V," in *2014 IEEE 26th International Symposium on Power Semiconductor Devices & IC's (ISPSD)* (IEEE, 2014) pp. 179–181.

¹⁴H. Cha, K. Lee, J. Lee, and T. Lee, "0.18 μm 100 V-rated BCD with Large Area Power LDMOS with Ultra-low Effective Specific Resistance," in *2016 28th International Symposium on Power Semiconductor Devices and IC's (ISPSD)* (IEEE, 2016) pp. 423–426.

¹⁵A. Saadat, M. L. Van de Put, H. Edwards, and W. G. Vandenberghe, "LDMOS Drift Region With Field Oxides: Figure-of-Merit Derivation and Verification," *IEEE Journal of the Electron Devices Society* **10**, 361–366 (2022).

¹⁶A. Saadat, M. L. Van de Put, H. Edwards, and W. G. Vandenberghe, "Simulation Study on the Optimization and Scaling Behavior of LDMOS Transistors for Low-voltage Power Applications," *IEEE Transactions on Electron Devices* **67**, 4990–4997 (2020).

¹⁷A. Huang, "New Unipolar Switching Power Device Figures of Merit," *IEEE Electron Device Letters* **25**, 298–301 (2004).

¹⁸*International Roadmap for Devices and Systems (IRDS)* (Institute of Electrical and Electronics Engineers (IEEE), 2022).

¹⁹R. Garnett, *Bayesian Optimization* (Cambridge University Press, 2023).

²⁰P. I. Frazier, "A Tutorial on Bayesian Optimization," arXiv preprint arXiv:1807.02811 (2018).

²¹J. Bergstra and Y. Bengio, "Random Search for Hyper-parameter Optimization," *Journal of machine learning research* **13** (2012).

²²J. Snoek, H. Larochelle, and R. P. Adams, "Practical Bayesian Optimization of Machine Learning Algorithms," *Advances in neural information processing systems* **25** (2012).

²³J. Bergstra, R. Bardenet, Y. Bengio, and B. Kégl, "Algorithms for Hyper-parameter Optimization," *Advances in neural information processing systems*

- tems **24** (2011).
- ²⁴B. J. Shields, J. Stevens, J. Li, M. Parasram, F. Damani, J. I. M. Alvarado, J. M. Janey, R. P. Adams, and A. G. Doyle, "Bayesian Reaction Optimization as a Tool for Chemical Synthesis," *Nature* **590**, 89–96 (2021).
- ²⁵W. Xu, Z. Liu, R. T. Piper, and J. W. Hsu, "Bayesian Optimization of Photonic Curing Process for Flexible Perovskite Photovoltaic Devices," *Solar Energy Materials and Solar Cells* **249**, 112055 (2023).
- ²⁶A. Gaonkar, H. Valladares, A. Tovar, L. Zhu, and H. El-Mounayri, "Multi-Objective Bayesian Optimization of Lithium-Ion Battery Cells for Electric Vehicle Operational Scenarios," *Electronic Materials* **3**, 201–217 (2022).
- ²⁷S. Guan and N. Fu, "Class Imbalance Learning with Bayesian Optimization Applied in Drug Discovery," *Scientific Reports* **12**, 2069 (2022).
- ²⁸P.-J. Chuang, A. Saadat, M. L. Van De Put, H. Edwards, and W. G. Vandenberghe, "Algorithmic Optimization of Transistors Applied to Silicon LDMOS," *IEEE Access* **11**, 64160–64169 (2023).
- ²⁹S. J. S. Chelladurai, K. Murugan, A. P. Ray, M. Upadhyaya, V. Narasimharaj, and S. Gnanasekaran, "Optimization of Process Parameters Using Response Surface Methodology: A Review," *Materials Today: Proceedings* **37**, 1301–1304 (2021).
- ³⁰J. P. Kleijnen, "Design Of Experiments: Overview," in *2008 Winter Simulation Conference* (2008) pp. 479–488.
- ³¹J. R. Gardner, M. J. Kusner, Z. E. Xu, K. Q. Weinberger, and J. P. Cunningham, "Bayesian Optimization with Inequality Constraints," in *ICML*, Vol. 2014 (2014) pp. 937–945.
- ³²*Sentaurus User Guide* (Synopsys, 2016).
- ³³T. C. Lik, "The Effect of H₃PO₄ Processing on LDMOS Gate oxide Integrity in PolySilicon Buffered LOCOS," in *2017 28th Annual SEMI Advanced Semiconductor Manufacturing Conference (ASMC)* (2017) pp. 226–229.
- ³⁴R. Van Overstraeten and H. De Man, "Measurement of the Ionization Rates in Diffused Silicon *pn* Junctions," *Solid-State Electronics* **13**, 583–608 (1970).
- ³⁵J. Wei, Z. Ma, X. Luo, C. Li, G. Deng, H. Song, K. Dai, Y. Jia, D. Liao, S. Zhang, and B. Zhang, "Experimental Study of Ultralow On-resistance Power LDMOS with Convex-shape Field Plate Structure," in *2021 33rd International Symposium on Power Semiconductor Devices and ICs (ISPSD)* (2021) pp. 87–90.
- ³⁶K. N. Kaushal and N. R. Mohapatra, "A Zero-Cost Technique to Improve ON-State Performance and Reliability of Power LDMOS Transistors," *IEEE Journal of the Electron Devices Society* **9**, 334–341 (2021).
- ³⁷Z. Dong, B. Duan, C. Fu, H. Guo, Z. Cao, and Y. Yang, "Novel Idmos optimizing lateral and vertical electric field to improve breakdown voltage by multi-ring technology," *IEEE Electron Device Letters* **39**, 1358–1361 (2018).
- ³⁸D. P. Bertsekas, *Constrained Optimization and Lagrange Multiplier Methods* (Academic press, 2014).
- ³⁹J. van der Pol, A. Ludikhuizen, H. Huizing, B. van Velzen, R. Huetting, J. Mom, G. van Lijnschoten, G. Hessels, E. Hooghoudt, R. van Huizen, M. Swanenberg, J. Egbers, F. van den Elshout, J. Koning, H. Schlichtenhorst, and J. Soeteman, "A-BCD: An economic 100 V RESURF silicon-on-insulator BCD technology for consumer and automotive applications," in *12th International Symposium on Power Semiconductor Devices & ICs. Proceedings (Cat. No.00CH37094)* (2000) pp. 327–330.
- ⁴⁰B. Yi and X. Chen, "A 300 V Ultra Low Specific On Resistance High-side *p* LDMOS with Auto-biased *n*-LDMOS for SPIC," *IEEE Transactions on Power Electronics* **32**, 551–560 (2016).
- ⁴¹Y. K. Wakabayashi, T. Otsuka, Y. Krockenberger, H. Sawada, Y. Taniyasa, and H. Yamamoto, "Stoichiometric Growth of SrTiO₃ Films via Bayesian Optimization with Adaptive Prior Mean," *APL Machine Learning* **1** (2023).
- ⁴²S. Greenhill, S. Rana, S. Gupta, P. Vellanki, and S. Venkatesh, "Bayesian Optimization for Adaptive Experimental Design: A Review," *IEEE access* **8**, 13937–13948 (2020).
- ⁴³J. Chen, M. B. Alawieh, Y. Lin, M. Zhang, J. Zhang, Y. Guo, and D. Z. Pan, "Automatic Selection of Structure Parameters of Silicon on Insulator Lateral Power Device Using Bayesian Optimization," *IEEE Electron Device Letters* **41**, 1288–1291 (2020).
- ⁴⁴B. Kim and M. Shin, "Bayesian Optimization of MOSFET Devices Using Effective Stopping Condition," *IEEE Access* **9**, 108480–108494 (2021).
- ⁴⁵V. Macary, T. Sicard, and R. Petrutiu, "A Novel LDMOS Structure with High Negative Voltage Capability for Reverse Battery Protection in Automotive IC's," in *Proceedings of the 2000 BIPOLAR/BiCMOS Circuits and Technology Meeting (Cat. No. 00CH37124)* (IEEE, 2000) pp. 90–93.
- ⁴⁶C. Jeong, S. Myung, I. Huh, B. Choi, J. Kim, H. Jang, H. Lee, D. Park, K. Lee, W. Jang, J. Ryu, M.-H. Cha, J. M. Choe, M. Shim, and D. S. Kim, "Bridging TCAD and AI: Its Application to Semiconductor Design," *IEEE Transactions on Electron Devices* **68**, 5364–5371 (2021).
- ⁴⁷F. Reif and S. A. Rice, "Fundamentals of Statistical and Thermal Physics," *Physics Today* **20**, 85–87 (1967).